VOL. 14, NO. 23, DECEMBER 2019 ISSN 1819-6608
ARPN Journal of Engineering and Applied Sciences

www.arpnjournals.com

# INHERENT CHARACTERISTICS OF SPURIOUS OSCILLATION IN THE SOLUTION OF SCALAR CONVECTION-DOMINATED PROBLEM

Aslam Abdullah
Department of Aeronautical Engineering, Faculty of Mechanical and Manufacturing Engineering,
Universiti Tun Hussein Onn Malaysia, Parit Raja, Batu Pahat, Johor, Malaysia
E-Mail: aslam@uthm.edu.my

**ABSTRACT**

Various cases of scalar convection-dominated equation have been investigated by lots of researchers not only for its applications in many engineering problems, but also as test cases to improve the understanding in the other two aspects; firstly, in the testing of a numerical scheme, and secondly, in the analysis of numerical issues in the solution itself. In this paper, we consider the last aspect. In particular, we investigate the cases involving different Dirichlet boundary conditions when the scalar convection-dominated flow is steady, as well as transient flow. Such investigation focuses on spurious oscillation in the solution of the equation. The oscillation is first modelled by means of Fourier series. Then we take a closer look into the oscillation's characteristics in each individual case. We show that some of the characteristics is inherent in each case. The criteria to avoid such oscillation is verified against the solution itself, and some apparent anomalies are identified.

**Keywords:** convection-diffusion equations, finite difference method, spurious oscillation, grid number, tridiagonal matrix algorithm.

## 1. INTRODUCTION

The generic conservation equation in the partial differential form in Cartesian coordinates and tensor notation following the Einstein convention is given by

$$\partial_t(\rho\varphi) + \partial_{x_j}(\rho u_j\varphi) - \partial_{x_j}\left(\epsilon\partial_{x_j}\varphi\right) - s_\varphi = 0, \quad (1)$$

where $\rho$ is the density, $\varphi$ is the conserved property, $u_j$ are velocity components of the fluid in the axes directions at the point $(x_1, x_2, x_3)$ at time $t$, $\epsilon$ is the diffusivity of $\varphi$, and $s_\varphi$ is the source or sink of $\varphi$. Navier-Stokes equations, which have special features of mass and momentum conservations, are extensions of this equation.
Equation (1) takes the simplified form

$$D_t(\rho\varphi) - \partial_{x_j}\left(\epsilon\partial_{x_j}\varphi\right) = 0, \quad (2)$$

when zero source/sink is assumed. The first term in (2) is called the substantial derivative

$$D_t(\rho\varphi) = \partial_t(\rho\varphi) + \partial_{x_j}(\rho u_j\varphi). \quad (3)$$

The physical interpretation of the substantial derivative $D_t(\rho\varphi)$ is the time rate of change in $(\rho\varphi)$ following a moving fluid element. The first and second terms on the RHS of (3) are called the local derivative $\partial_t(\rho\varphi)$ (i.e. the physical change in $(\rho\varphi)$ with time at a fixed position), and the convective derivative $\partial_{x_j}(\rho u_j\varphi)$ (i.e. the physical change in $(\rho\varphi)$ with time due to the mass transfer and change in its properties from one spatial position to another), respectively. Substituting (3) into (2) we have

$$\partial_t(\rho\varphi) + \partial_{x_j}(\rho u_j\varphi) - \partial_{x_j}\left(\epsilon\partial_{x_j}\varphi\right) = 0. \quad (4)$$

Equation (4) is further simplified in the case of the fluids at rest, or of small velocity $(u_j \approx 0)$, or large diffusivity $\epsilon$, as well as solids as

$$\partial_t(\rho\varphi) - \partial_{x_j}\left(\epsilon\partial_{x_j}\varphi\right) = 0,$$

representing the pure diffusion process where the local derivative $\partial_t(\rho\varphi)$ is balanced by the diffusive derivative $\partial_{x_j}\left(\epsilon\partial_{x_j}\varphi\right)$.For more details, see [1].

We take both the steady and unsteady one-dimensional conservation equation with and without the source, involving the scalar whose concentration is denoted by $\varphi$ into account. Such scalar is carried along with the moving fluid element (convection) and spreads due to diffusion. Given appropriate boundary conditions, it can be shown that at relatively high velocity $u$, or low diffusivity $\epsilon$, the scalar concentration $\varphi$either initially grows slowly in space and then suddenly rises over a defined distance, orthe scalar concentration $\varphi$profile skewed in the direction of increasing defined distance. We define (1) that fulfills these conditions to be scalar convection-dominated equation SCDE. The sudden growth of $\varphi$or high skew of $\varphi$ profile not only provides a severe test of the discretization method, but also in the selection of compatible grid structure over the computation domain. Note that the solution of (1) is either linearin space or symmetric when $u$ is negligible, which is not our interest here.

We establish the relationship between the flow parameter of interest (i.e. the Peclet number $Pe$) in SCDE and the appropriate grid number $N$in the case of steady flow, and between$Pe$ and time $t$in the case of unsteady flow, by formulating the criteria which are necessary in achieving physically accurate solution of the equation, thus unify the deduction of heuristic selections of $N$or $Pe$for solving the contaminated fluids problem that leads

to less pre-computation time. Note that inappropriate pair of $Pe$ and $N$ results in numerical oscillation [2] as illustrated in Figure-1. The work presented in this paper follows the line initiated in [2] and [3] for defining the sequence of both low Peclet numbers $Pe$ and grid numbers $N$.

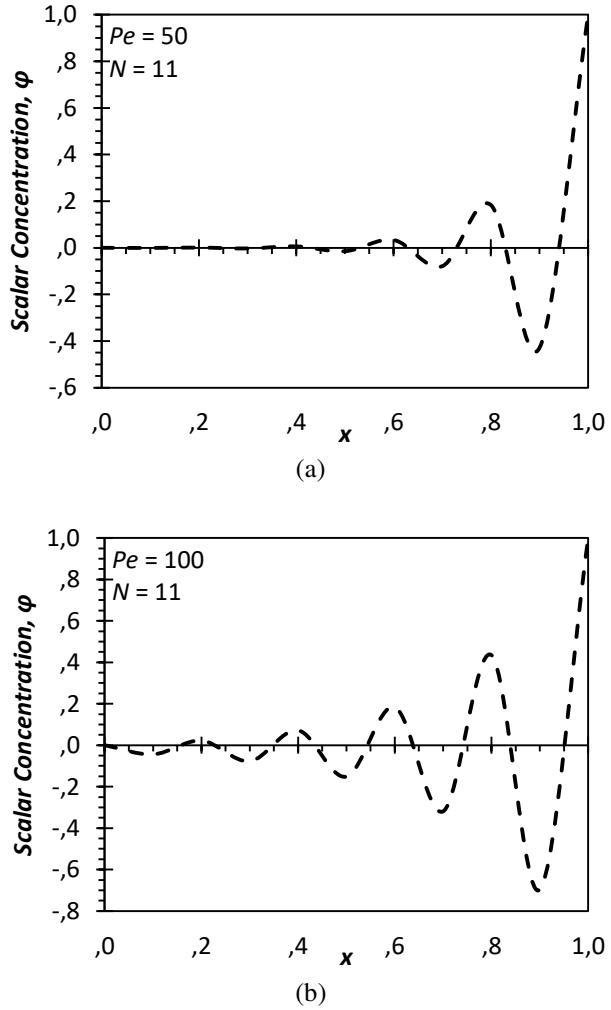


**Figure-1.** Nonphysical behaviour of scalar concentration profile$\varphi$due to the insufficient grid number in computational domain.

We consider three cases. Case I involves steady SCDE with the following Dirichlet boundary conditions; $\varphi(0) = 0$ and $\varphi(1) = 0$. Case II differs from Case I only with respect to the boundary conditions where $\varphi(0) = \varphi(1) = 0$. The last case (i.e. Case III) is that where unsteady SCDE is considered with the same boundary conditions as in Case I.

## 2. CONVECTION-DOMINATED PROBLEMS

A wide range of numerical methods for solving convection-dominated equation CDE are by now well formulated and many useful schemes can be found such as finite divergences, finite elements, spectral procedures, and the method of lines[4]-[14]. For instance, [4] presented a comparative study between two most popular Lattice Boltzmann (LB) models for CDE (i.e. those in two dimensions with five and nine discrete lattice velocities, respectively). Other variants include multiple-relaxation-time LB model for the axisymmetric, as well as isotropic and anisotropic diffusion processes whose both applicability and accuracies have been investigated by [5] and [6] respectively. In the problem where no scalar or flux jump exists, [7] introduced a numerical scheme for dealing with curved interfaces with second-order spatial accuracy in conjunction with the LB method.

Bittl *et al.* [8] summarized well-known a priori error estimates for the discontinuous Galerkin approximation which carry over to the subspace of the discontinuous piecewise-quadratic space, while [9] proposed the approximation of high order alternating evolution.

Zhang *et al.* [10] claimed that the fourth-order compact difference scheme requires only 15 grid points to solve CDE, while [11] successfully proved that it is computationally more efficient than the standard second-order central difference scheme.

Current methods include those to solve nonlinear fractional CDE, as homotopy analysis transform and homotopy perturbation Sumudu transform techniques whose reliability and efficiency were clearly demonstrated in [12], and that based on the operational matrices of shifted Jacobi polynomials of high accuracy [13].

Martin [14] introduced a Schwarz waveform relaxation algorithm for the CDE that converges without overlap of the subdomains.

It is important to note that the choice of suitable computational grid to discretize the governing partial differential equations (e.g. by means of polynomial fitting, Taylor series expansion and compact scheme to obtain approximations to the derivatives of the variables with respect to the coordinates) is necessary at the onset of numerical modelling of the convection-dominated problems as in [4]-[15]. It is worth to note here that the variable values at locations other than the defined grid nodes can also be determined by interpolation. Another important aspect is the method to solve the discretized algebraic equations. The solution is obtained via either direct [16]-[18] or iterative [19]-[22] methods.

Another method, called the shooting method, is also used for determining convection-dominated flow properties [23]. Its variants are those of Goodman and Lance [24], parallel shooting method [25], Green's function and Gaussian quadrature based methods, Ritz's method [26], and Euler shooting method. In relatively complex problems, the method deals with non-linear property of the differential equations. A remark on this was given by [27], while [28] and [29] illustrated the relevant application in solving beam equation, and predicting convection-dominated flow, respectively. The method's advantages include the ability to prove the presence of kinks of, for instance, the extended Fischer-Kolmogorov equation [30] and the existence of multiple solutions in an indefinite Neumann problem [31]. Moreover, the method yields, in some cases, better results than those obtainable via fixed-point techniques [32].

Despite of the advantages, [26] highlighted general limitations of the shooting method.

We discretize SCDE on uniform grids, where the expansion factor $r_e = 1$. A Fourier series is utilized to model the spatial error resulting from either insufficient grid number or relatively higher Peclet number. The criteria for predicting $\varphi$ profile with out non-physical oscillation are then formulated.

## 3. SEQUENCES OFTHE PARAMETERS

The range of low Peclet numbers $Pe$ of interests is $[0,100]$. We define a sequence of $Pe$ by

$$\begin{aligned} &Pe_i, \\ &Pe_{i+1} = Pe_i/p, \\ &Pe_{i+2} = Pe_{i+1}/p, \\ &Pe_{i+3} = Pe_{i+2}/p, \\ &\cdot \\ &\cdot \\ &\cdot \\ &Pe_n = Pe_{n-1}/p, \end{aligned} \tag{5}$$

where the constants $i, p \in \mathbb{Z}^+$.
Defining a sequence of $N$ by

$$\begin{aligned} &N_i, \\ &N_{i+1} = floor\left(\frac{N_i + 1}{p}\right), \\ &N_{i+2} = floor\left(\frac{N_{i+1} + 1}{p}\right), \\ &N_{i+3} = floor\left(\frac{N_{i+2} + 1}{p}\right), \\ &\cdot \\ &\cdot \\ &\cdot \\ &N_n = floor\left(\frac{N_{n-1} + 1}{p}\right), \end{aligned} \tag{6}$$

where the constants $i, p \in \mathbb{Z}^+$.

Next, defining a sequence of normalized time $t$ by

$$\begin{aligned} &t_i, \\ &t_{i+1} = i\frac{k}{2p}t_i, \\ &t_{i+2} = (i+1)\frac{k}{2p}t_i, \\ &t_{i+3} = (i+2)\frac{k}{2p}t_i, \\ &\cdot \\ &\cdot \\ &\cdot \\ &t_{n-1} = (n-2)\frac{k}{2p}t_i, \end{aligned} \tag{7}$$

where $i, p \in \mathbb{Z}^+$ and $k$ is the the number of time step $\Delta t$ when the solution of (1) converges.

Let

$i = 1, n = 6, Pe_1 = 100, N_1 = 81, t_i = \Delta t, p = 2,$ such that the sequence in (5), (6), and (7) become

$100,50,25,12.5,6.25,3.125$ ;
$81, 41, 21, 11, 6, 3;$
$\Delta t, .25k\ \Delta t, 0.5k\ \Delta t, 0.75k\ \Delta t, k\ \Delta t,$

respectively. All 36 possible pairs $(Pe, N)$ and 30 pairs $(Pe, t)$ based on the elements in these sequences are considered as test cases, following the line used in [2] and [3]. The numerical solutions for such cases are presented in Figure-2, Figure-4(b).

## 4. INSTABILITY MODEL

Discretizing (1) by applying Crank-Nicolson method;

$$\frac{\varphi_i^{n+1} - \varphi_i^n}{\Delta t} = A + B + 1, \tag{8}$$

where

$$A = -\frac{1}{2\Delta x}\left(\frac{\varphi_{i+1}^{n+1} + \varphi_{i+1}^n}{2} - \frac{\varphi_{i-1}^{n+1} + \varphi_{i-1}^n}{2}\right),$$

$$B = \frac{\epsilon}{(\Delta x)^2}(C + D + E),$$

$$C = \frac{\varphi_{i+1}^{n+1} + \varphi_{i+1}^n}{2},$$

$$D = -\frac{2\varphi_i^{n+1} + 2\varphi_i^n}{2},$$

$$E = \frac{(\varphi_{i-1}^{n+1} + \varphi_{i-1}^n)}{2}.$$

Since Crank-Nicolson method is unconditionally time-stable, then the averaged $\varphi$at two different times may be suppressed and the change of $\varphi$ with respect to time may be ignored, in modeling the instability such that

$$A = -\frac{1}{2\Delta x}(\varphi_{i+1}^n - \varphi_{i-1}^n),$$

$$B = \frac{\epsilon}{(\Delta x)^2}(\varphi_{i+1}^n - 2\varphi_i^n + \varphi_{i-1}^n),$$

$$C = \varphi_{i+1}^n,$$

$$D = -2\varphi_i^n,$$

$$E = \varphi_{i-1}^n.$$

Thus (8) becomes

$$0 = \left(-\frac{\varphi_{i+1}^n - \varphi_{i-1}^n}{2\Delta x}\right) + \left(\epsilon \frac{\varphi_{i+1}^n - 2\varphi_i^n + \varphi_{i-1}^n}{(\Delta x)^2}\right) + 1.$$

For simplicity, we rewrite the last equation as

$$0 = \left(-\frac{\varphi_{i+1} - \varphi_{i-1}}{2\Delta x}\right) + \left(\epsilon \frac{\varphi_{i+1} - 2\varphi_i + \varphi_{i-1}}{(\Delta x)^2}\right) + 1. \quad (9)$$

The spatial error is defined as

$$\gamma = \mathcal{N} - E, \quad (10)$$

where $\mathcal{N}$ and $E$ are finite accuracy numerical solution from a real computer and exact solution of difference equation, respectively. Note that the numerical solution $\mathcal{N}$ satisfies the difference equation (9). A Fourier series model can be used to analytically represent the random variation of $\gamma$ with respect to space;

$$\gamma(x) = \sum_l e^{\alpha x} e^{ik_l x}, l = 1,2,3 \dots, \quad (11)$$

where $e^{\alpha x}$ is the amplification factor, $k_l$is the wave number, and $\alpha$ is a constant.

Lets $e^{\alpha x}$ in (11) be proportional to $x$ when numerical oscillation occurs. Thus it is sufficient to consider only the growth of $e^{\alpha x}$. Direct substitution of $e^{\alpha x}$ into the finite difference equation (11) gives

$$\frac{e^{\alpha(x+\Delta x)} - e^{\alpha(x-\Delta x)}}{2\epsilon} = \frac{e^{\alpha(x+\Delta x)} - 2e^{\alpha x} + e^{\alpha(x-\Delta x)}}{\Delta x}. \quad (12)$$

Divide (12) by $e^{\alpha x}$, we have

$$\frac{e^{\alpha\Delta x} - e^{-\alpha\Delta x}}{2\epsilon} = \frac{e^{\alpha\Delta x} - 2 + e^{-\alpha\Delta x}}{\Delta x},$$

which, after some rearrangement, becomes

$$e^{\alpha\Delta x} = \frac{e^{-\alpha\Delta x}(\Delta x + 2\epsilon) - 4\epsilon}{\Delta x - 2\epsilon}.$$

If $e^{\alpha x}$ presumably grows with respect to $x$, then

$$\frac{e^{\alpha(x+\Delta x)}}{e^{\alpha x}} > 1,$$

or simply

$$e^{\alpha\Delta x} > 1.$$

Therefore, in order to have non-growing error amplification, the criterion

$$\frac{e^{-\alpha\Delta x}(\Delta x + 2\epsilon) - 4\epsilon}{\Delta x - 2\epsilon} \leq 1 \quad (13)$$

must be fulfilled. Criterion (13) can also be expressed in term of both $N$ and $Pe$ for both Case I and Case II as follows:

$$\frac{e^{-\frac{\alpha}{N-1}}\left(\frac{1}{N-1} + \frac{2}{Pe}\right) - \frac{4}{Pe}}{\frac{1}{N-1} - \frac{2}{Pe}} \leq 1. \quad (14)$$

We define

$$G = \frac{e^{-\frac{\alpha}{N-1}}\left(\frac{1}{N-1} + \frac{2}{Pe}\right) - \frac{4}{Pe}}{\frac{1}{N-1} - \frac{2}{Pe}}. \quad (15)$$

Thus (14) becomes

$$G \leq 1. \quad (16)$$

Substituting $N = 11$as in Case III into (15);

$$G = \frac{e^{-0.1\alpha}\left(0.1 + \frac{2}{Pe}\right) - \frac{4}{Pe}}{0.1 - \frac{2}{Pe}} \quad (17)$$

The criterion in (17) is clearly a function of single variable $Pe$.

## 5. RESULTS OF CALCULATIONS

The criterion in (15) was checked against all 36 possible pairs$(Pe_i, N_i)$ in each Case I and Case IIbased on sequences (5) and (6). The criterion in (17) was checked against 30 pairs $(Pe_i, t_i)$ in Case III based on sequences (5) and (7). The output is given in Table-1 for Case I and Case II, and in Table-2 for Case III.

In Table-1, all grid numbers in sequence (14) are appropriate in achieving physically accurate non-oscillatory solutions if$Pe = 3.125$. This is indicated by$G$being less than or equal to 1. The appropriate range of $N$ shrinks by one element each time the next$Pe$in sequence (5) is considered.

Data in Table-2 indicate that the numerical results are physically accurate non-oscillatory ones (i.e. when $G \leq 1$) if the smallest three Peclet numbers of interest are considered. This information matches those in Table-1.

The values of $G$ tabulated in Table-1 and Table-2 were verified by plotting the concentration $\varphi$ which are numerically calculated for $Pe$ against $N$ and against $t$ as shown in Figure-2, Figure-3 and Figure-4(a), Figure-4(b), respectively.

It is confirmed now that in any case (i.e. Case I, Case II, or Case III) where $G > 1$ the numerical oscillations appear, and the amplitudes grow with respect to $x$. The only exception is $\varphi$ profiles when$N = 3$in Figure-3 which appear to be non-oscillating despite $G > 1$ as shown in Table-1. This will be further explained in the next section.

**Table-1.** Range of grid numbers $N$ that fulfils to the criterion in (23) as in Case I and Case II, where $\alpha = -0.1$. The shaded cells indicate cases where $G > 1$, while the double outlined cells are also applicable for Case III.

| ***Pe* = 3.125** | | ***Pe* = 6.25** | | ***Pe* = 12.5** | | ***Pe* = 25** | | ***Pe* = 50** | | ***Pe* = 100** | |
|---|---|---|---|---|---|---|---|---|---|---|---|
| ***N*** | ***G*** | ***N*** | ***G*** | ***N*** | ***G*** | ***N*** | ***G*** | ***N*** | ***G*** | ***N*** | ***G*** |
| 81 | $\leq 1$ | 81 | $\leq 1$ | 81 | $\leq 1$ | 81 | $\leq 1$ | 81 | $\leq 1$ | 81 | $\leq 1$ |
| 41 | | 41 | | 41 | | 41 | | 41 | | 41 | $> 1$ |
| 21 | | 21 | | 21 | | 21 | | 21 | $> 1$ | 21 | |
| 11 | | 11 | | 11 | | 11 | $> 1$ | 11 | | 11 | |
| 6 | | 6 | | 6 | $> 1$ | 6 | | 6 | | 6 | |
| 3 | | 3 | $> 1$ | 3 | | 3 | | 3 | | 3 | |

**Table-2.** Peclet numbers $Pe$, and $G$ as in criterion (19) where $\alpha = -0.1$, for Case III. The shaded cells indicate situations where the spurious oscillations appear.

| ***Pe*** | ***G*** |
|---|---|
| 3.125 | $\leq 1$ |
| 6.25 | |
| 12.5 | |
| 25 | $> 1$ |
| 50 | |
| 100 | |

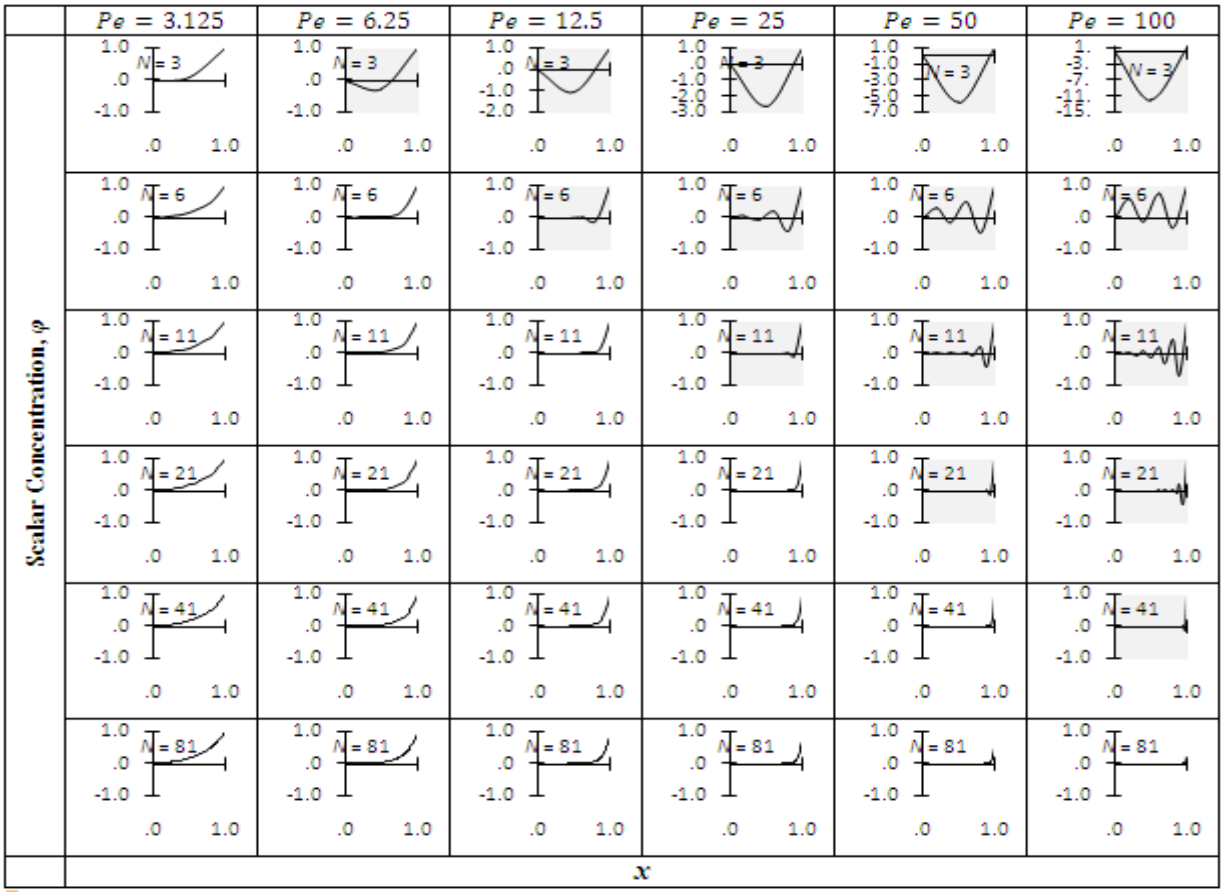


**Figure-2.** Case I. Concentration profile $\varphi$ at $Pe$ and $N$ as in sequences (5) and (6), respectively. The shaded plots indicate cases where the numerical oscillations appear.

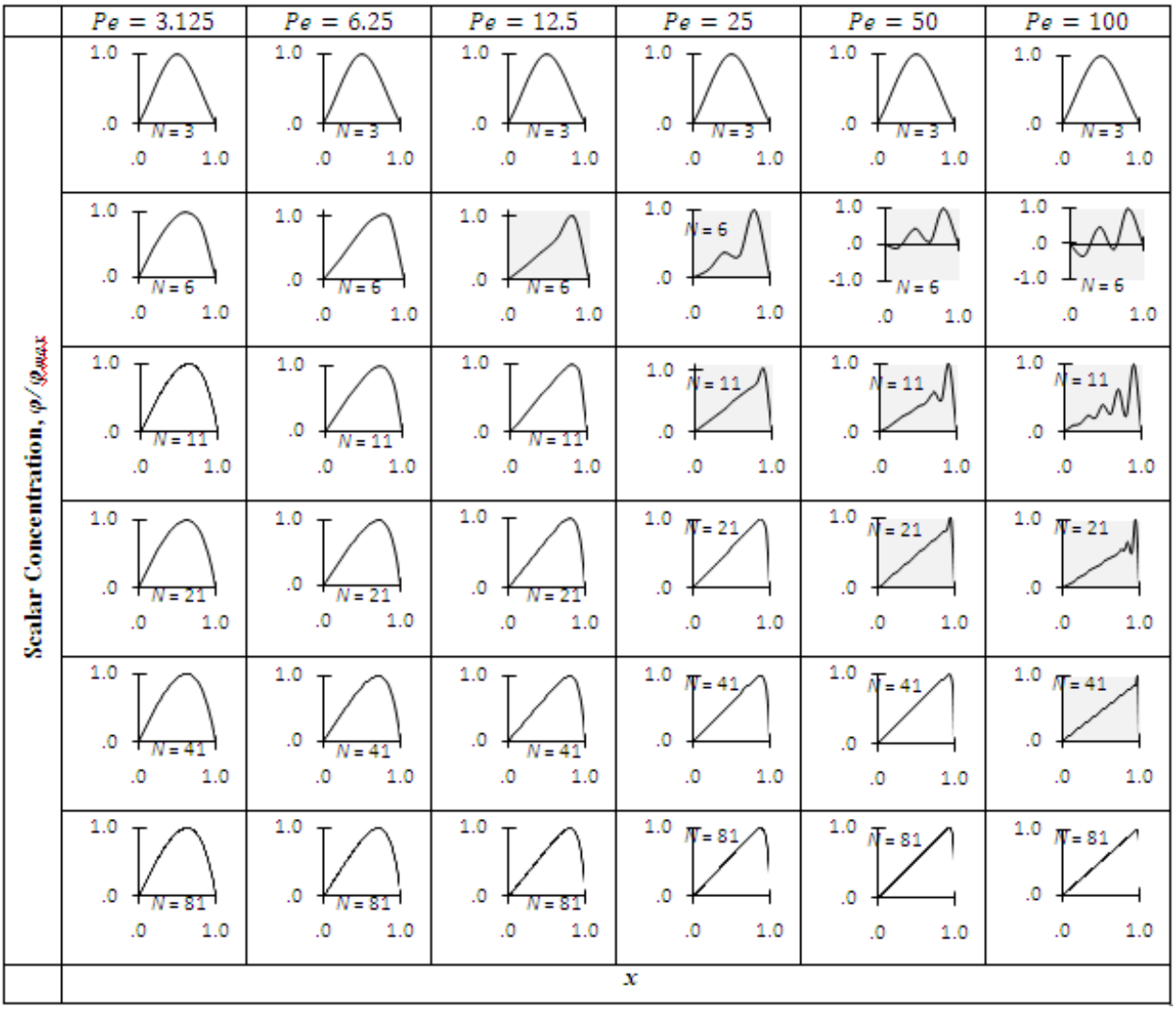


**Figure-3.** Case II. Concentration profile $\varphi/\varphi_{max}$ at $Pe$ and $N$as in sequences (5) and (6), respectively. The shaded plots indicate cases where the numerical oscillations appear.

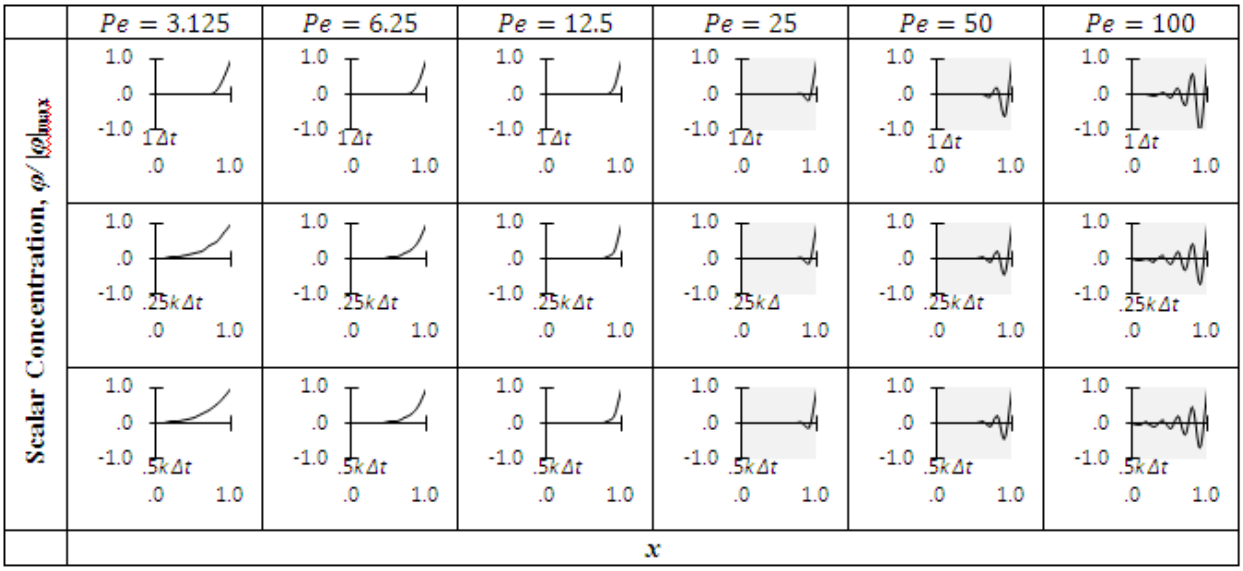


**Figure-4(a).** Case III. Concentration profile $\varphi/|\varphi|_{max}$ at $Pe$as in sequence (5) and $t = \Delta t, .25k\ \Delta t, 0.5k\ \Delta t$as in sequences (7). The shaded plots indicate cases where the spurious oscillations appear.

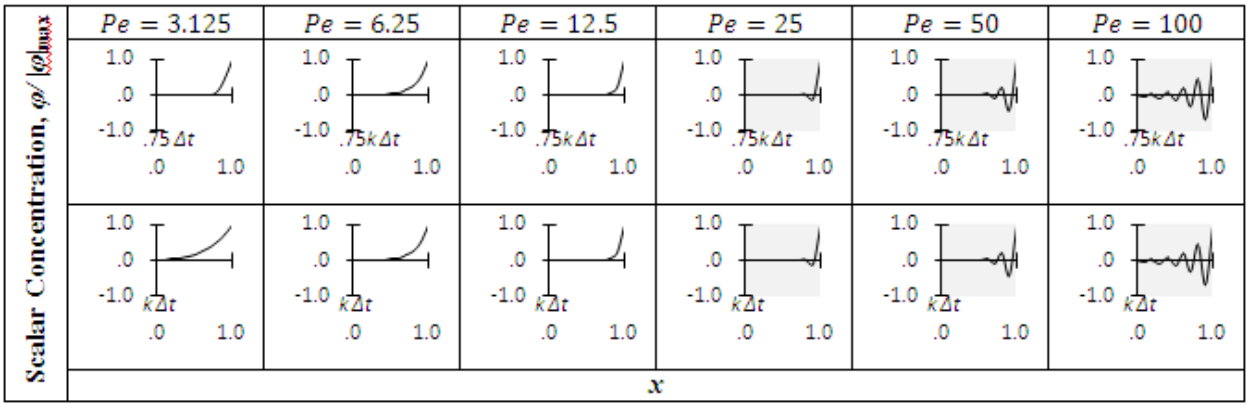


**Figure-4(b).** Case III. Concentration profile $\varphi/|\varphi|_{max}$ at $Pe$ as in sequence (5) and $t = .75k\ \Delta t, k\ \Delta t$ as in sequences (7).$t = .75k\ \Delta t, k\ \Delta t$. The shaded plots indicate cases where the spurious oscillations appear.

It is interesting to note that the numerical oscillations which appear in shaded plots in Figure-2, Figure-4(b) begin with a kink. These kinks are representatively highlighted further in Figure-5 for better visual understanding. The only exception is $\varphi$ profiles when$N = 3$in Figure-2 which appear to have no kink at all despite $G > 1$for $Pe = 6.25,12.5, \ldots ,100$as shown in Table-1(a). This will be further explained in the next section.

It is obvious that, as depicted in Figure-2, Figure-4(b), spurious oscillations occur at certain $Pe$, irrespective whether the flow is steady (i.e. Case I and

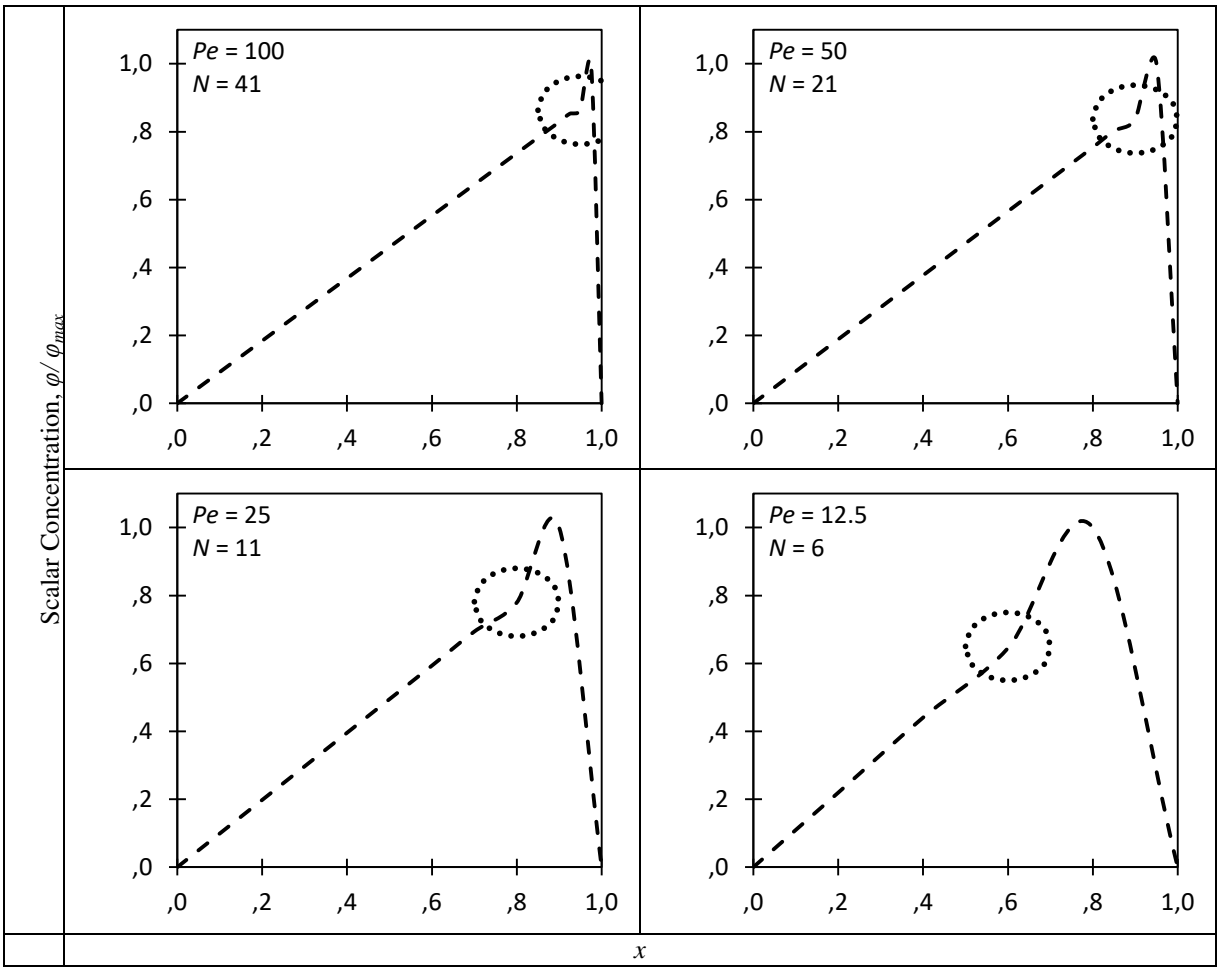


**Figure-5.** Concentration profile $\varphi/\varphi_{max}$ with clearer kinks which mark the beginning of the spurious oscillations at next $Pe$sequence. The kinks are marked by the circles.

Case II) or unsteady (i.e. Case III). In other words, such oscillations are time independant.

Furthermore, the amplitudes grow with respect to $x$ as discussed in§4.

Note the area under the curve represented by the integral

$$\int_0^1 \varphi(x)\, dx$$

is inversely proportional to $Pe$ in all cases I, II, and III.

## 6. CONCLUSIONS

A technique in predicting spurious oscillations in the solutions of SCDE is highlighted. The key aspect in this research is the modelling of spatial error growth which results from the discretization technique. This opens the possibility of a more general framework for the selection of numerical scheme in computational fluid dynamics, and the relationship between the flow parameter/s and the solution quality in finite difference method.

Criteria in (15)-(17) represent a qualitative guideline that improves our understanding on;

a) The contribution of pair $(Pe, N)$ to the oscillation, in Case I and Case II. The criteria also give the nominal values of $N$ below which non-physical solutions occur. This illustrates the influence of $(Pe, N)$.

b) The influence of Peclet number, $Pe$, rather than time, $t$, on the physically accurate results, in Case III.

These two aspects form a basis for a relatively more effective approach in solving SCDE. It is found that the criteria are able to capture the presence of kinks which mark the beginning of the oscillations. It is this capability that explains the anomaly involves$\varphi$ profile at $(Pe, N) = (6.25,3), (12.5,3), \ldots, (100,3)$ in Case I as can be seen in Figure-2 where there is no kink detected despite the presence of oscillation and $G > 1$. Even though the oscillations are generally preceded by a kink, it is impossible to capture it in an exponential curve of three points (i.e. $N = 3$).

Another interesting anomaly is in Case II involving $\varphi$ profile at $(Pe, N) = (6.25,3)$ in Figure-3 where there is neither kink nor oscillation despite $G > 1$. It is thus impossible to capture both in a polynomial curve of three points (i.e. $N = 3$).

Finally, we found that in the case of unsteady SCDE (i.e. Case III), the numerical error patterns, in particular those of oscillations are qualitatively identical with respect to time. Such patterns are clearly observable in Figure-4. The only influence on the pattern comes from $Pe$. Note that in this case, $N$ is kept constant (i.e. $N$=11).

## ACKNOWLEDGEMENT

The author would like to thank Universiti Tun Hussein Onn Malaysia (UTHM) and Ministry of Education of Malaysia (MOE) for the research facilities.

## REFERENCES

[1] Abdullah A. 2018. Formulation of low Peclet number based grid expansion factor for the solution of convection-diffusion equation. Eng. Technol. Appl. Sci. Res. 8: 2680-2684.

[2] Abdullah A. 2018. Mathematical relationship between grid and low Peclet numbers for the solution of convection-diffusion equation. ARPN J. Eng. Appl. Sci. 13(9): 3182-3187.

[3] Abdullah A. 2018. Obtaining grid number for the shooting method solution of convection-diffusion equation.International Journal of Mechanical Engineering, & Technology (IJMET). 9(5): 916-924.

[4] Li L., Mei R. and Klausner J. 2017. Lattice Boltzmann models for the convection-diffusion equation: D2Q5 vs D2Q9. Int. J. Heat Mass Transf. 108: 41-62.

[5] Li L., Mei R. and Klausner J. 2013. Multiple-relaxation-time lattice Boltzmann model for the axisymmetric convection diffusion equation. Int. J. Heat Mass Transf. 67: 338-351.

[6] Hu Y., Li D., Shu S. and Niu X. 2016. Lattice Boltzmann flux scheme for the convection-diffusion equation and its applications. Comput. Math. with Appl. 72(1): 48-63.

[7] Hu Z., Huang J., Huang W. and Cui G. 2017. Second-order curved interface treatments of the lattice Boltzmann method for convection-diffusion equations with conjugate interfacial conditions. Comput. Fluids. 144: 60-73.

[8] Bittl M., Kuzmin D. and Becker R. 2014. The CG1-DG2 method for convection-diffusion equations in 2D. J. Comput. Appl. Math. 270: 21-31.

[9] Liu H. and Pollack M. 2016. Alternating evolution discontinuous Galerkin methods for convection-diffusion equations. J. Comput. Phys. 307: 574-592.

[10] Zhang J., Ge L. and Kouatchou J. 2000. A two colorable fourth-order compact difference scheme and parallel iterative solution of the 3D convection

diffusion equation. Math. Comput. Simul. 54(1-3): 65-80.

[11] Sun H., Kang N., Zhang J. and Carlson E. 2003. A fourth-order compact difference scheme on face centered cubic grids with multigrid method for solving 2D convection diffusion equation. Math. Comput. Simul. 63(6): 651-661.

[12] Singh J., Swroop R. and Kumar D. 2016. A computational approach for fractional convection-diffusion equation via integral transforms. Ain Shams Eng. J. 1-10.

[13] Behroozifar M. and Sazmand A. 2017. An approximate solution based on Jacobi polynomials for time-fractional convection-diffusion equation. Appl. Math. Comput. 296: 1-17.

[14] Martin V. 2005. An optimized Schwarz waveform relaxation method for the unsteady convection diffusion equation in two dimensions. Appl. Numer. Math. 52(4): 401-428.

[15] Tian Z. and Yu P. 2011. A high-order exponential scheme for solving 1D unsteady convection-diffusion equations. J. Comput. Appl. Math. 235(8): 2477-2491.

[16] Biringen S. 1981. A note on the numerical stability of the convection-diffusion equation. J. Comput. Appl. Math. 7(1): 17-20.

[17] Zhai S., Feng X. and He Y. 2014. An unconditionally stable compact ADI method for three-dimensional time-fractional convection-diffusion equation. J. Comput. Phys. 269: 138-155.

[18] Zhou Z. and Liang D. 2017. The mass-preserving and modified-upwind splitting DDM scheme for time-dependent convection-diffusion equations. J. Comput. Appl. Math. 317: 247-273.

[19] Ge L. and Zhang J. 2001. High accuracy iterative solution of convection-diffusion equation with boundary layers on nonuniform grids. J. Comput. Phys. 171(2): 560-578.

[20] Ma Y. and Ge Y. 2010. A high order finite difference method with Richardson extrapolation for 3D convection-diffusion equation. Appl. Math. Comput. 215(9): 3408-3417.

[21] Mohamed S., Mohamed N., Gawad A. and Matbuly M. 2013. A modified diffusion coefficient technique for the convection diffusion equation. Appl. Math. Comput. 219(17): 9317-9330.

[22] Boret S. and Jimnez O. 2017. Integrated framework for solving the convection-diffusion equation on 2D Quad mesh relying on internal boundaries. Comput. Math. with Appl. 74(1): 218-228.

[23] Abdullah A. 2019. Grid expansion factor for the shooting method solution of convection-diffusion equation. ARPN J. Eng. Appl. Sci. 14(7): 1370-1376.

[24] Roberts S. and Shipman J. 1967. Continuation in shooting methods for two-point boundary value problems. J. Math. Anal. Appl. 18: 45-58.

[25] Marzulli P. 1991. Global error estimates for the standard parallel shooting method. J. Comput. Appl. Math. 34(2): 233-241.

[26] Ha S. 2001. A nonlinear shooting method for two-point boundary value problems. Comput. Math. with Appl. 42(10-11): 1411-1420.

[27] Hieu N. 2003. Remarks on the shooting method for nonlinear two-point boundary-value problems. VNU J. Sci. 3: 18-25.

[28] Amster P. and Alzate P. 2008. A shooting method for a nonlinear beam equation Nonlinear Anal. Theory Methods Appl. 68(7): 2072-2078.

[29] Rehman K. and Malik M. 2017. Application of shooting method on MHD thermally stratified mixed convection flow of non-Newtonian fluid over an inclined stretching cylinder. IOP Conf. Ser. J. Phys. 822: 1-12.

[30] Peletier L. and Troy W. 1996. A Topological shooting method and the existence of kinks of the extended Fischer-Kolmogorov equation. Topl. Methods Nonlinear Anal. 6: 331-355.

[31] Feltrin G. and Sovrano E. 2018. Three positive solutions to an indefinite Neumann problem: a shooting method. Nonlinear Anal. Theory, Methods Appl. 166: 87-101.

[32] Kwong M. 2006. The shooting method and multiple solutions of two/multi-point BVPs of second-order ODE Electron. J. Qual. Theory Differ. Equations. 6: 1-14.